DOI: 10.1002/asia.200800253

Density Functional Studies on Thromboxane Biosynthesis: Mechanism and Role of the Heme-Thiolate System

Tetsuya K. Yanai and Seiji Mori*[a]

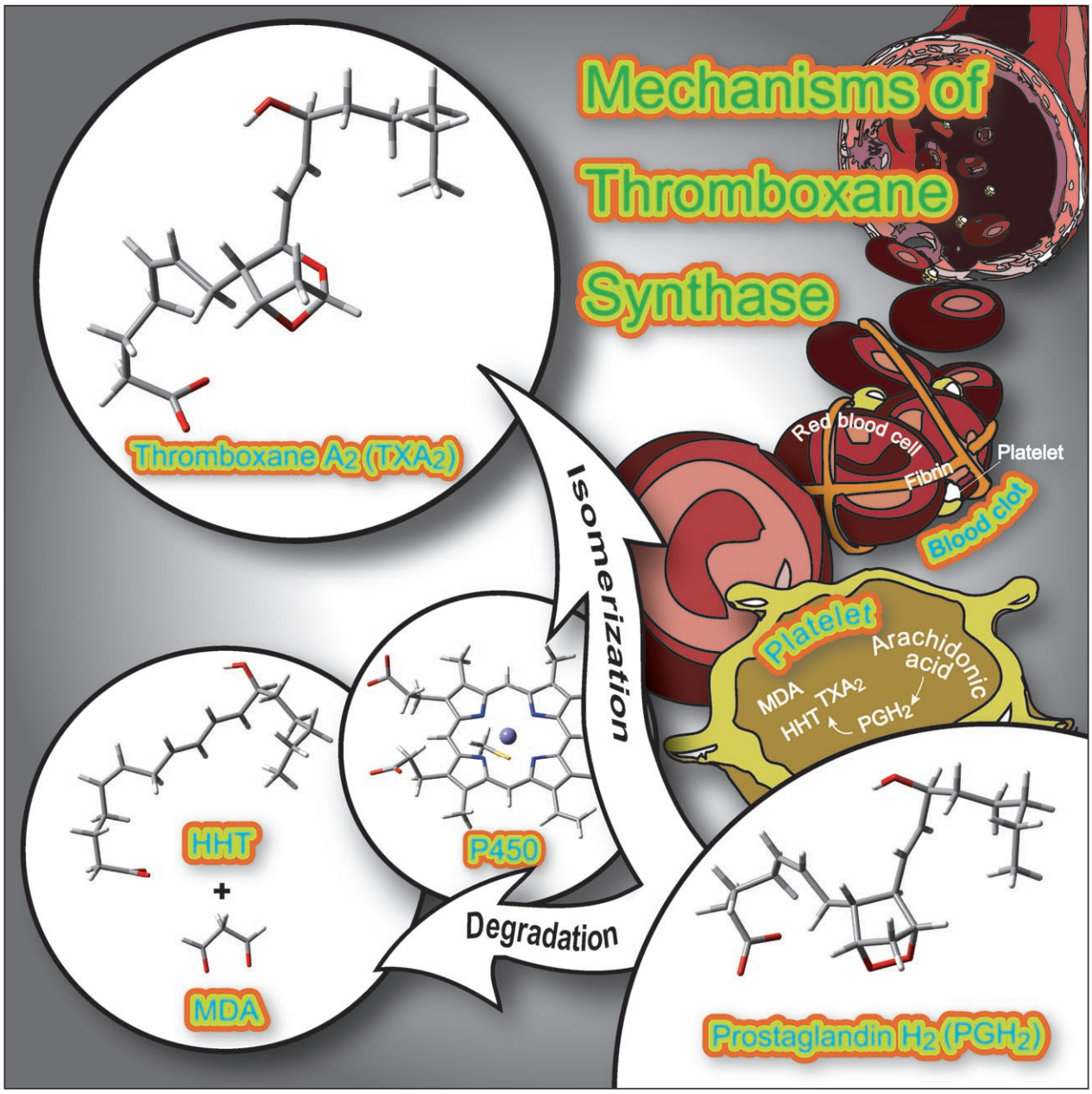

Abstract: Reaction mechanisms for the isomerization of prostaglandin H_2 to thromboxane A_2, and degradation to 12-L-hydroxy-5,8,10-heptadecatrienoic acid (HHT) and malondialdehyde (MDA), catalyzed by thromboxane synthase, were investigated using the unrestricted Becke-three-parameter plus Lee–Yang–Parr (UB3LYP) density functional level theory. In addition to the reaction pathway through Fe^{IV}-porphyrin intermediates, a new reaction pathway through Fe^{III}-porphyrin π-cation radical intermediates was found. Both reactions proceed with the homolytic cleavage of endoperoxide O–O to give an alkoxy radical. This intermediate converts into an allyl radical intermediate by a C–C homolytic cleavage, followed by the formation of thromboxane A_2 having a 6-membered ring through a one electron transfer, or the degradation into HHT and MDA. The proposed mechanism shows that an iron(III)-containing system having electron acceptor ability is essential for the 6-membered ring formation leading to thromboxane A_2. Our results suggest that the step of the endoperoxide O–O homolytic bond cleavage has the highest activation energy following the binding of prostaglandin H_2 to thromboxane synthase.

Keywords: cytochromes · density functional calculations · isomerization · peroxides · prostaglandins

Introduction

Thromboxane A_2 (TXA_2) and prostacyclin (PGI_2) are arachidonic acid metabolites. TXA_2 is a potent mediator of platelet aggregation, vasoconstriction, and bronchoconstriction,[1] whereas PGI_2 is a potent mediator of platelet anti-aggregation and vasodilation.[2] In addition, these mediators are also related to diabetes mellitus and arrhythmias, and play a key role in cardiovascular and pulmonary diseases.[3] TXA_2 and PGI_2 are produced from prostaglandin H_2 (PGH_2) using thromboxane synthase (TXAS) and prostacyclin synthase (PGIS), respectively, which are members of the cytochrome P450 (P450) superfamily[4,5] (Scheme 1). Nonenzymatic hydrolysis of TXA_2 and PGI_2 leads to more stable compounds, thromboxane B_2 (TXB_2) and 6-keto-prostaglandin $F_{1\alpha}$ (6-keto-$PGF_{1\alpha}$, respectively. TXB_2 is produced in a molar ratio of 1:1:1 with two other breakdown products of PGH_2, that is, 12-L-hydroxy-5,8,10-heptadecatrienoic acid (HHT) and malondialdehyde (MDA).[6] The molar ratio varies depending on the reaction condition.[7]

The P450 superfamily has a heme-thiolate moiety as its catalytic center (Figure 1). This enzyme group has a variety of functions including drug metabolism and steroid biosynthesis. Many studies have been conducted on this group of enzymes because of their important medical and biological functions.[8] Typical reactions catalyzed by P450s are monooxygenation reactions,[8,9] which require an oxygen donor, and electrons from reductases. TXA_2 and PGI_2 biosyntheses by TXAS and PGIS, respectively, are classified as isomerization reactions that are unusual among the reactions catalyzed by P450. Interestingly, despite low amino acid se-

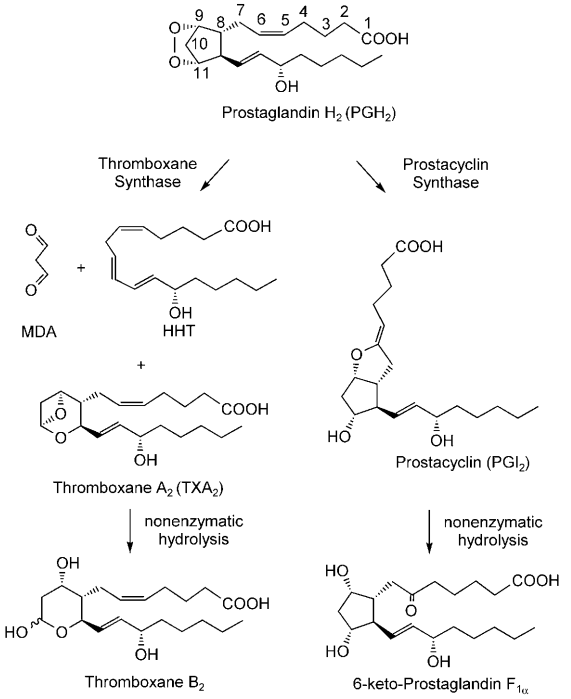

Scheme 1. Conversion of prostaglandin H_2 into thromboxane A_2, degradation to HHT and MDA by thromboxane synthase, and conversion into prostacyclin by prostacyclin synthase.

[a] T. K. Yanai, Prof. Dr. S. Mori
Faculty of Science
Ibaraki University
Bunkyo, Mito 310-8512 (Japan)
Fax: (+81) 29-228-8403
E-mail: smori@mx.ibaraki.ac.jp

Supporting information for this article is available on the WWW under http://dx.doi.org/10.1002/asia.200800253.

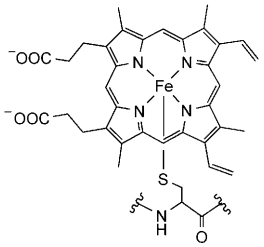

Figure 1. Heme-thiolate, Fe^{III}-protoporphyrin IX with a cysteinate as an axial ligand, is an active center of cytochrome P450.

quence identity (16%) between human TXAS and bovine PGIS,[10] both enzymes catalyze isomerization reactions from the same substrate, PGH_2. Moreover their products, TXA_2 and PGI_2, have opposing actions.

Since TXA_2 was discovered to be a potent mediator for platelet aggregation,[11] many studies on TXA_2 and TXAS have been conducted,[12] and hypothetical mechanisms were reported.[13–15] One is an Fe^{II}-catalyzed mechanism proposed by Turner and Herz,[13] and another is an ionic O–O bond cleavage mechanism by a proton proposed by Diczfalusy and Hammarström.[14] However, at that time, there had been little information about what TXAS was, until it became clear that TXAS was a member of the cytochrome P450 superfamily, and that TXA_2 biosynthesis was not catalyzed by Fe^{II} but by Fe^{III}-porphyrin.[15] A reaction mechanism of TXA_2 biosynthesis has been proposed by Hecker and Ullrich based on experiments with PGH_2 analogues and [5,6,8,9,11,12,14,15-^{2}H] PGH_2 (Scheme 2).[15] First, the endoperoxide oxygen atom at C(9) attaches to the heme iron(III) of TXAS (**i**). EPR, resonance Raman, and UV/Vis spectroscopic studies showed that a TXAS–PGH_2 analogue complex has a hexacoordinate low-spin heme.[15–17] The mechanism proceeds with the homolytic cleavage of the PGH_2 endoperoxide O–O bond, resulting in a hexacoordinate Fe^{IV}-porphyrin intermediate (**ii**) with an alkoxy radical. This is followed by β-scission of the alkoxy radical yielding products with a carbon-centered radical (**iii**). Finally, the substrate forms a zwitterion (**iv**) by one electron transfer from the carbon-centered radical to the heme-iron to give TXA_2, or alternatively, decomposes into HHT and MDA.

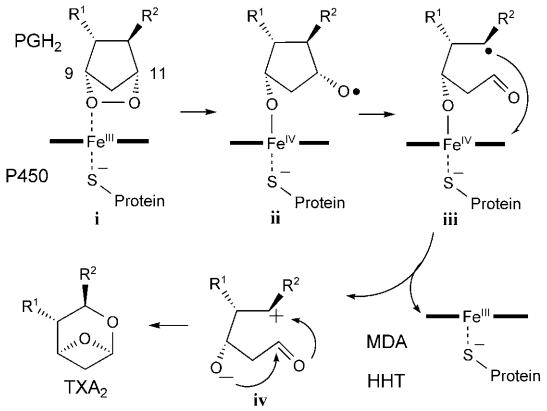

Scheme 2. Previously proposed reaction mechanism of TXA_2 biosynthesis. (R^1: $CH_2CH{=}CHC_2H_6COOH$, R^2: $CH{=}CHCHOHC_5H_{11}$). See Ref. [15].

Homolytic and heterolytic cleavage of the O–O bond of peroxides are reactions of relevance to P450 chemistry and organometallic chemistry.[18,19] Both TXAS and PGIS favor the homolytic cleavage of the O–O bond based on the reactions with 10-hydroperoxyoctadeca-8,12-dienoic acid and 15-hydroperoxyeicosatraenoic acid.[20,21] The kinetics for PGH_2 and its analogues, suggest that the rate-limiting step for TXA_2 biosynthesis is not the isomerization process (Scheme 2) but the substrate-binding step of TXAS.[22]

A number of studies by mutagenesis analyses and homology modelling have been published for predicting the three-dimensional TXAS structure.[23,24] However, the crystal structure of TXAS is not available at the moment, although X-ray structures were determined for human and zebra fish PGISs.[25] Magnetic circular dichroism and EPR analyses showed that TXAS has a more hydrophobic distal heme pocket than those in classical P450s.[16]

Although many experiments for TXAS have been reported, the reactive intermediates are difficult to detect. Therefore, the details of the fast isomerization process of TXA_2 biosynthesis remain obscure. The role of the iron-porphyrin system in TXA_2 biosynthesis and in its decomposition into HHT and MDA has not yet been established. Although the proposed mechanism by Hecker and Ullrich is rational,[15] a reaction pathway that considers the Fe^{III}-porphyrin π-cation radical intermediates has not been proposed in mechanistic studies of TXA_2 biosynthesis. The redox change from Fe^{III} to Fe^{IV} after the O–O bond cleavage of PGH_2 could not be observed in the EPR spectrum of TXAS catalyzed PGH_2 isomerization.[22] Hence, in this study, we have investigated the isomerization mechanism for TXA_2 biosynthesis and the role of the iron(III)-porphyrin system using models of P450 (**A**), PGH_2 (**B**), TXA_2 (**C**), and HHT (**D**) (Figure 2), using the unrestricted Becke-three-parameter plus Lee–Yang–Parr (UB3LYP) density functional level of theory.[26] Theoretical studies on oxidation mechanisms of hydroxylation,[27–30] ep-

Abstract in Japanese:

トロンボキサン合成酵素によるプロスタグランジンH_2のトロンボキサンA_2への異性化反応、及び12-L-ヒドロキシ-5,8,10-ヘプタデカトリエン酸(HHT)とマロンジアルデヒド(MDA)への分解反応の反応機構についてUB3LYP密度汎関数法を用いて検討した。検討の結果、Fe^{IV}–ポルフィリン中間体を通る経路とFe^{III}–ポルフィリン–π–カチオンラジカル中間体を経由する経路が見つかった。両方の経路ともエンドペルオキシドのO–O結合ホモリティック開裂により始まり、アルコキシラジカルを形成する。このアルコキシラジカル中間体はC–C結合ホモリティック開裂によりアリルラジカルに変わる。その後、一電子移動を伴った六員環形成反応が起こればトロンボキサンA_2が生成し、六員環を形成しないとHHTとMDAへ分解する。今回の検討により、一電子受容能を持つFe^{III}–ポルフィリン錯体がトロンボキサンA_2に至る六員環中間体の形成に必要であることがわかった。また、プロスタグランジンH_2がトロンボキサン合成酵素に配位した後の律速段階がエンドペルオキシドのO–O結合ホモリティック開裂であることがわかった。

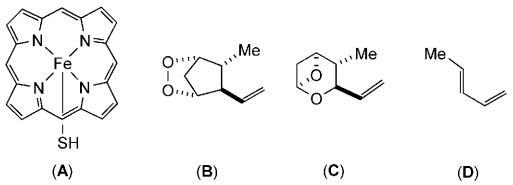

Figure 2. Models of TXAS (**A**), PGH_2 (**B**), TXA_2 (**C**), and HHT (**D**).

oxidation,[31,32] sulfoxidation,[33] and *N*-demethylation,[34] and on the mechanism of N–N bond formation in the presence of NO reductase[35] by the model of P450, have contributed significantly to the improvement in P450 science.[36] The present studies are the first theoretical studies for isomerization reactions catalyzed by cytochrome P450.

Results and Discussion

In order to examine the role of the Fe^{III}-porphyrin system in thromboxane A_2 biosynthesis, we investigated reaction mechanisms of the isomerization of PGH_2 to TXA_2 both in the presence and absence of the iron porphyrin, and compared them. BII and BI basis sets are described in the Computational Method section.

Isomerization in the Absence of Iron-Porphyrin

The isomerization reaction mechanism of PGH_2 model **B**, to TXA_2 model **C**, in the absence of the iron porphyrin **A** at the UB3LYP/BII//UB3LYP/BI level was investigated. Both singlet and triplet spin states are considered. The spin states are symbolized as a symbol for the species with a number in the upper left (for example, singlet: ^{1}**X**, triplet: ^{3}**X**). The optimized structures of singlet and triplet reaction intermediates, and the transition states of isomerization from ^{1}**B** to ^{1}**C** are illustrated in Figure 3. All potential energy profiles are summarized in Figure 4.

First, the homolytic cleavage of the O(1)–O(2) bond in singlet endoperoxide ^{1}**B** leads to the singlet alkoxy radical intermediate ^{1}**1** through the transition state ^{1}**TS1**. Along with this process, the spin densities of O(1) and O(2) change from 0.00 and 0.00 in ^{1}**B** to −0.78 and 0.81 in ^{1}**1**, respectively. The spin localizations on O(1) and O(2) in ^{1}**1** indicate that the formation of alkoxy radicals is homolytic. The formation of the open-shell singlet alkoxy radical intermediate ^{1}**1** occurs with an activation energy of 86.5 kJ mol^{-1}. The triplet alkoxy radical ^{3}**1** lies lower in energy than the singlet intermediate ^{1}**1** by 1.2 kJ mol^{-1} (Figure 4).

In the second step, a β-scission of alkoxy radical O(2) in the triplet intermediate ^{3}**1** leads to an allyl radical ^{3}**2** through a transition state ^{3}**TS2** with an activation energy of 12.2 kJ mol^{-1} (Figure 4). The singlet transition state ^{1}**TS2** and the intermediate ^{1}**2** cannot be located because of the spontaneous fragmentation to products, **MDA** and **D**. Although there would be conical intersections between singlet and triplet potential energy surfaces, we cannot properly locate the points using B3LYP functional theory. A zwitterionic intermediate of **2**, previously proposed by Hecker and Ullrich[15] (**iv** in Scheme 2), cannot be located at the

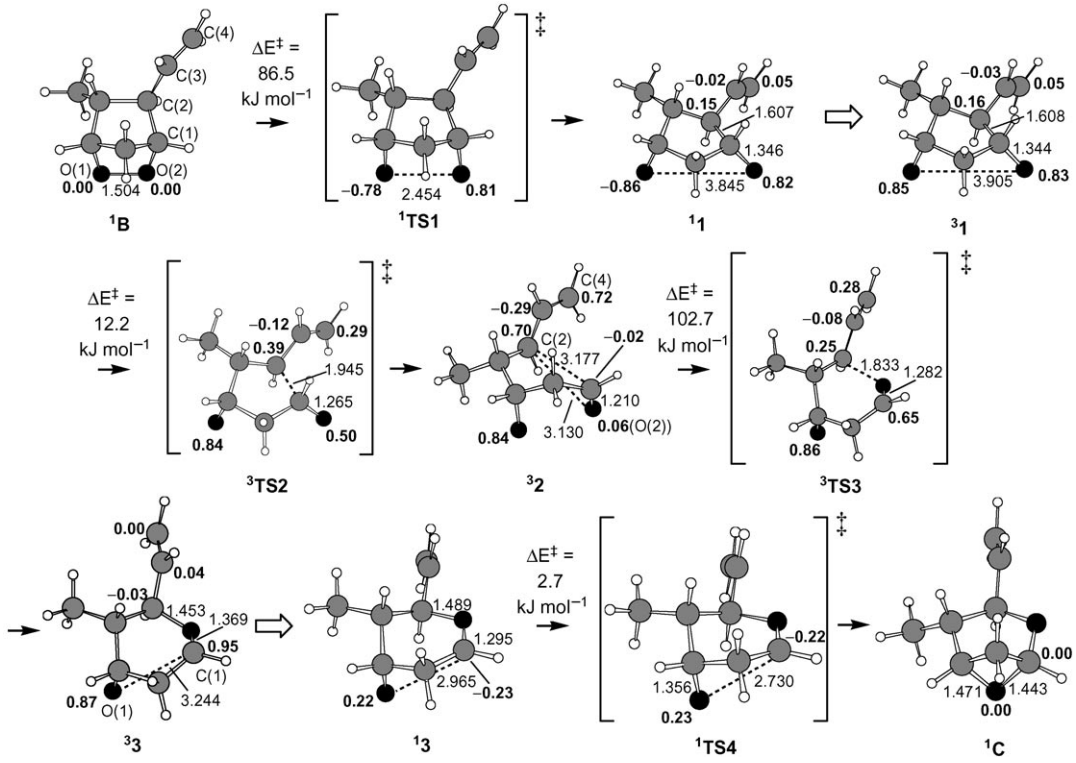

Figure 3. Optimized structures of the formation of TXA_2 model (**C**) from PGH_2 model (**B**) for the singlet and triplet states at the UB3LYP/BI level. Distances are in angstrom. Activation energies are at the UB3LYP/BII//UB3LYP/BI level. Numbers in bold are spin densities.

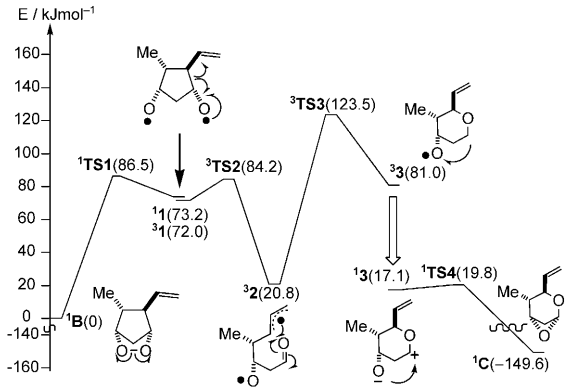

Figure 4. Energy profiles of the formation of TXA_2 model (**C**) from PGH_2 model (**B**) for the singlet and triplet states in the absence of **A**. Energies are in kJ mol^{-1} at the UB3LYP/BII//UB3LYP/BI level.

UB3LYP/BII, UB3LYP/BI, and UB3LYP(CPCM)/BII levels, leads to fragmentation products **MDA**, and a model of HHT **D** (Figure 5a). The explicit water coordination to the zwitterion **2** does not change the conclusion (Figure 5b).

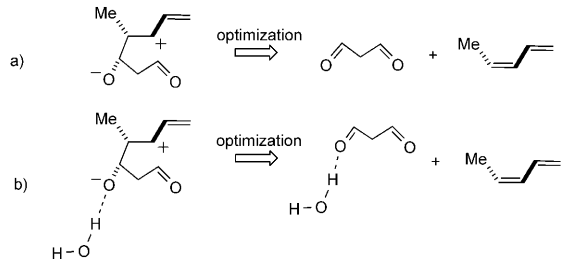

Figure 5. Trials for geometry optimizations of zwitterionic intermediate at the UB3LYP/BII, UB3LYP/BI, and UB3LYP(CPCM)/BII levels.

In the third step, the allyl radical intermediate ^{3}**2** forms a 6-membered ring intermediate including a carbon radical ^{3}**3**, by the binding of the carbonyl oxygen O(2) to the allyl carbon C(2) (Figure 3). The decrease of spin densities on the allyl radical C(2) and C(4) atoms from 0.70 and 0.72 to −0.03 and 0.00, and the increase of spin density on the carbonyl carbon atom C(1) from −0.02 to 0.95, show that the formation of the six-membered ring proceeds by a radical coupling bond formation between O(2) and C(2) atoms with an activation energy of 102.7 kJ mol^{-1}. This high activation energy implies that the six-membered ring formation occurs neither in the gas phase nor without catalyst. An optimization of singlet 6-membered biradical intermediate leads to a cationic intermediate ^{1}**3**, which is lower in energy by 63.9 kJ mol^{-1} than ^{3}**3** (Figure 4). Finally, the zwitterion ^{1}**3** forms the TXA_2 model ^{1}**C** with ionic rearrangement, and proceeds with a low activation energy of 2.7 kJ mol^{-1}.

Isomerization in the Presence of the Iron-Porphyrin System

To examine the role of the Fe^{III}-porphyrin system in the thromboxane biosynthesis, we investigated several electronic structures for a model reaction mechanism of PGH_2 isomerization catalyzed by P450, and compared the catalytic reaction using iron-porphyrin with the noncatalytic reaction. It is known that hydroxylation and epoxidation reactions, including hexacoordinate iron-porphyrin species, favor doublet or quartet reaction pathways.[28,30,37] Our results show comparable differences in the energetics. Hence, the following discussion describes primarily the structures for the doublet reaction pathway. However details of structures of quartet intermediates are provided in the Supporting Information.

The optimized structures of doublet reaction intermediates, transition states of isomerization from **B** to **C**, and transition states of degradation to MDA and **D** are illustrated in Figure 6. All potential energy profiles are summarized in Figure 7. In Figure 6 and 7, spin states are symbolized as a symbol for the species with a number in the upper left (for example, doublet: ^{2}**X**, quartet: ^{4}**X**, sextet: ^{6}**X**). In the pentacoordinate Fe^{III}-porphyrin **A**, the sextet state ^{6}**A** is lower in energy than the doublet state ^{2}**A** and the quartet state ^{4}**A** by 29.3 kJ mol^{-1} and 9.0 kJ mol^{-1}, respectively (Figure 7). It is consistent with experimental evidence for sextet high-spin pentacoordinate TXAS.[5,15] In the first step, the endoperoxide O(1) of the substrate **A** coordinates with the Fe atom in the formation of a hexacoordinate Fe^{III} complex, ^{2}**4**. The quartet state of the iron-porphyrin complex ^{4}**4** is degenerate with ^{2}**4**. Experimental observation shows the doublet low-spin for hexacoordinate TXAS complexes with PGH_2 or its analogues.[5,17,22,38] In the sextet state ^{6}**4**, the Fe–O(1) distance of 2.868 Å was located (structural data are provided in the Supporting Information). Compared to an X-ray Fe–OH_2 distance of 2.28 Å for a resting $P450_{cam}$,[39] the Fe–O(1) distance is too long for ^{6}**4** to be a hexacoordinate complex. In addition, the iron-porphyrin ^{6}**A** is stabilized with only 1.3 kJ mol^{-1} by interaction with ^{1}**B**. One can conclude that ^{6}**4** is still a pentacoordinate system, and predict that much weaker interaction occurs between the sextet cytochrome P450 and PGH_2 than the doublet and quartet P450s. The homolytic cleavage of the O(1)–O(2) bond of ^{2}**4** leads to the intermediate ^{2}**5^{IV}** through the transition state ^{2}**TS5^{IV}**. Along with this process, the negative spin density of O(2) increases from 0.00 in ^{2}**4** to −0.82 in ^{2}**5^{IV}**. The spin localization on O(2) in ^{2}**5^{IV}** indicates the formation of an alkoxy radical as well as an increase in the O(2) negative spin density. The increase of spin density number on Fe from 1.26 to 2.07, and the increase of positive charge from +0.99 to +1.10, indicate that Fe is oxidized from Fe^{III} to Fe^{IV}. These results indicate that the O(1)–O(2) bond cleavage is homolytic, and that the Fe–O(1) bond length decreases as Fe^{III} oxidises to Fe^{IV}. The formation of the alkoxy radical intermediate ^{2}**5^{IV}** occurs with an activation energy of 52.5 kJ mol^{-1}, which is much lower than the 86.5 kJ mol^{-1} required for ^{1}**1** formation (see above). These results indicate that the Fe^{III}-porphyrin system reduces the activation energy of the O–O bond cleavage by 34.0 kJ mol^{-1}.

For the comparison of several electronic configurations, we examined the doublet pathway leading to the doublet Fe^{III}-porphyrin π-cation radical intermediate ^{2}**5^{III}** (Figure 8)

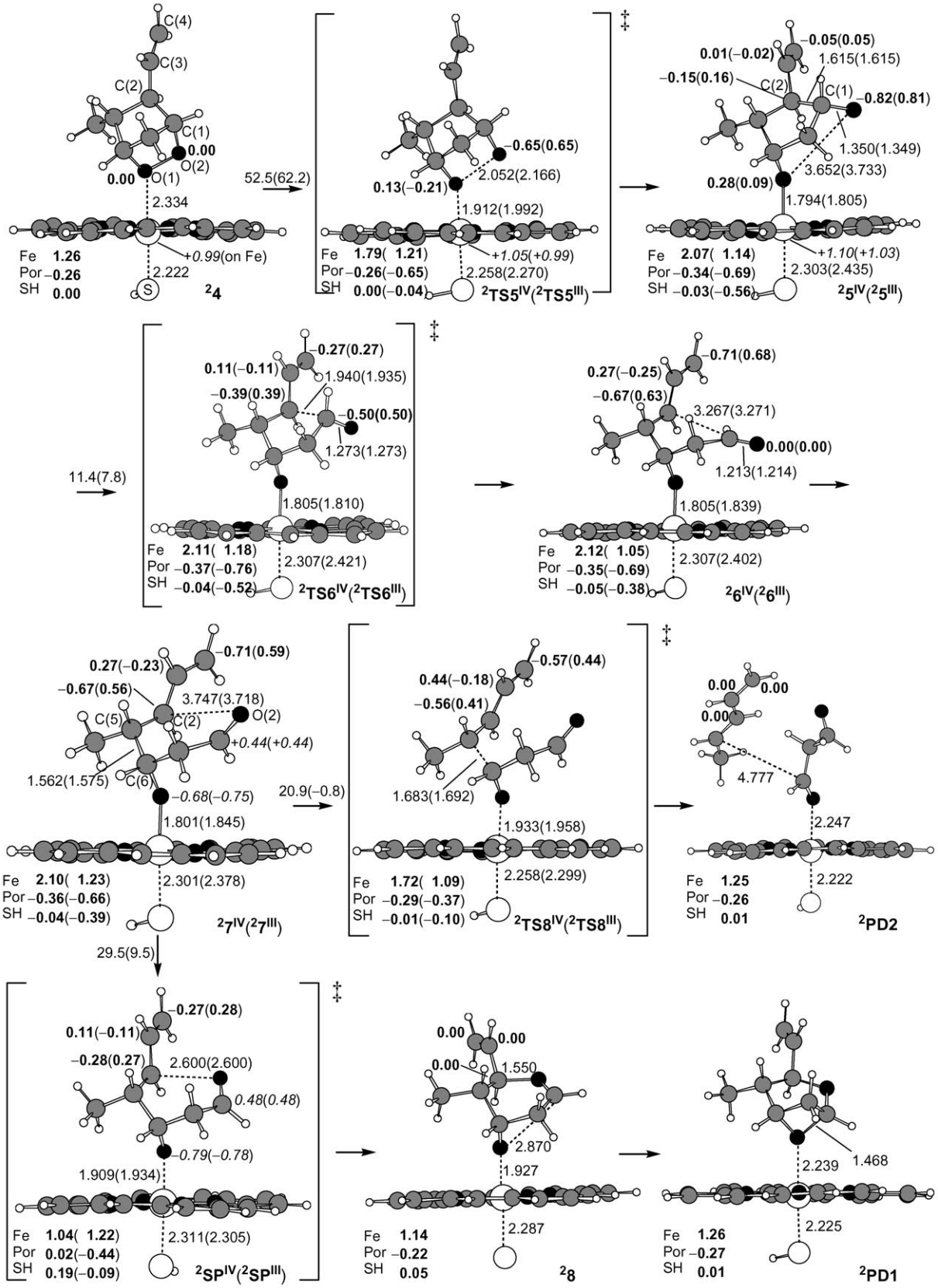

Figure 6. Optimized structures at the UB3LYP/BI level on the pathway through doublet Fe^{IV} intermediates and on the pathway through doublet Fe^{III}-porphyrin π-cation radical intermediates. Data for the Fe^{III} pathway are in parentheses. Distances are in angstrom. Activation energies are in kJ mol^{-1} at the UB3LYP/BII//UB3LYP/BI level. Numbers in bold and in italics are calculated spin densities and natural charges at the UB3LYP/BII//UB3LYP/BI level, respectively.

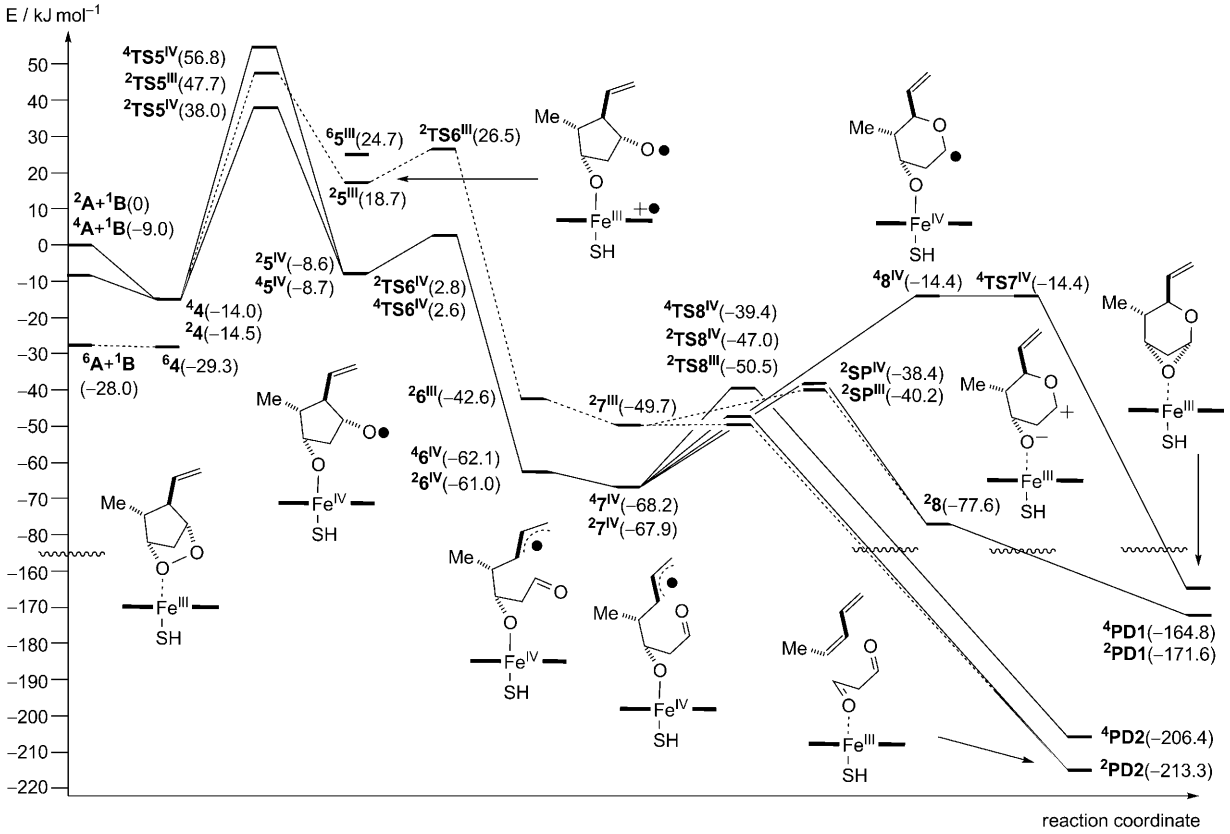

Figure 7. Energy profiles of the formation of TXA_2 model (**C**) from PGH_2 model (**B**) by P450 model (**A**) for the doublet state. Energies are at the UB3LYP/BII//UB3LYP/BI level in kJ mol^{-1} relative to the sum of energies for ^{2}**A** and ^{1}**B**.

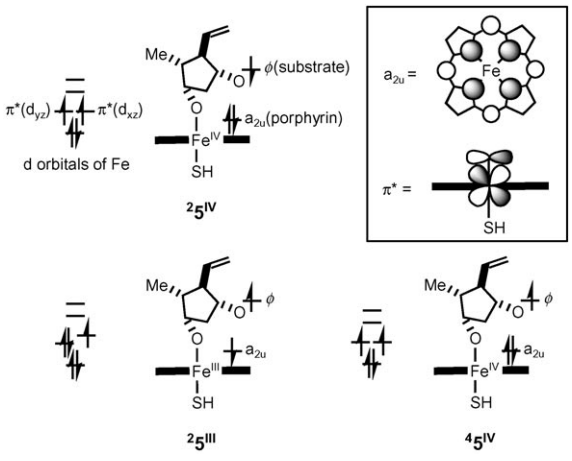

Figure 8. Electronic structures of the doublet Fe^{IV}-porphyrin complex (^{2}**5**^{IV}), the doublet Fe^{III}-porphyrin π-cation radical complex (^{2}**5**^{III}) and the quartet Fe^{IV}-porphyrin complex (^{4}**5**^{IV}).

through the transition state ^{2}**TS5**^{III}, and the quartet pathway leading to the Fe^{IV} intermediate ^{4}**5**^{IV} (Figure 8) through the transition state ^{4}**TS5**^{IV}. In Figure 8, ϕ and a_{2u} refer to a singly occupied orbital for the substrate and a high-lying occupied orbital for the porphyrin moiety, respectively. In the present paper, these electronic structures are symbolized as a complex symbol with a Roman numeral in the upper right (for example, Fe^{IV}-porphyrin: **X**^{IV}, Fe^{III}-porphyrin π-cation radical: **X**^{III}). These electronic structures were determined based on analyses of calculated spin densities, and Kohn–Sham molecular orbitals.

In the doublet Fe^{III} pathway, the activation energy for the formation of ^{2}**5**^{III} is 62.2 kJ mol^{-1} (Figure 6 and 7). The spin density on Fe does not change very much (from 1.26 in ^{2}**4** to 1.14 in ^{2}**5**^{III}), whereas the negative spin density on the porphyrin moiety increases from −0.26 to −0.69 by loss of one electron from the a_{2u} orbital. These results indicate the formation of the Fe^{III}-porphyrin π-cation radical in ^{2}**5**^{III}. The activation energy for the ^{4}**5**^{IV} formation is 70.8 kJ mol^{-1} (Figure 7). The activation energies for the ^{2}**5**^{III} and ^{4}**5**^{IV} formations are higher than that for ^{2}**5**^{IV} formation, which is 52.5 kJ mol^{-1}. These results show that the homolytic cleavage of the O–O bond proceeds mainly through the transition state ^{2}**TS5**^{IV}. The Fe^{IV} intermediates, ^{2}**5**^{IV} and ^{4}**5**^{IV}, are more stable than the Fe^{III}-porphyrin π-cation radical intermediate ^{2}**5**^{III} by ~27 kJ mol^{-1}. The most stable sextet intermediate, ^{6}**5**^{III}, is higher in energy by 33.3 kJ mol^{-1} than ^{2}**5**^{IV}. Note that we cannot locate ^{6}**5**^{IV} because of its instability. The previous DFT studies on hydroxylation also showed that hexacoordinate sextet intermediates are much higher in energy than the doublet and quartet intermediates.[30]

To investigate the effect of vinyl groups in the heme-thiolate complex on the energy gap of the Fe^{IV}-porphyrin and

Fe^{III}-porphyrin π-cation radical complexes, we also calculated hexacoordinate complexes, $^{2}\mathbf{5}^{\mathbf{IV}}$**(vinyl)**, containing two vinyl groups at the UB3LYP/BII//UB3LYP/BI level. A small energy difference of 0.2 kJ mol^{-1} for the relative energies between the Fe^{IV} and the Fe^{III}-porphyrin π-cation radical complexes is found (Figure 9).

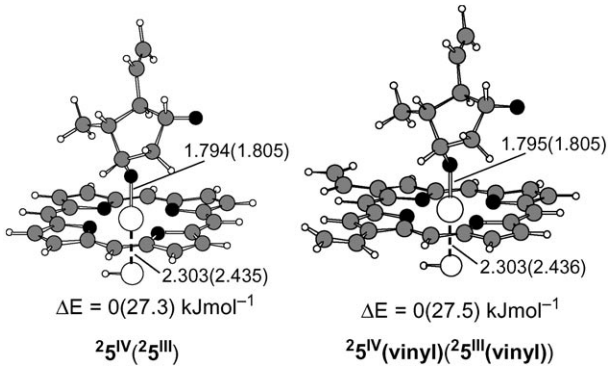

Figure 9. Optimized structures of alkoxy radical intermediates at the UB3LYP/BI level and relative energies at the UB3LYP/BII//UB3LYP/BI level.

In the second step (Figure 6), the alkoxy radical $^{2}\mathbf{5}^{\mathbf{IV}}$ converts to an allyl radical $^{2}\mathbf{6}^{\mathbf{IV}}$ with C(1)−C(2) bond cleavage through the transition state $^{2}\mathbf{TS6}^{\mathbf{IV}}$ with an activation energy of 11.4 kJ mol^{-1}. This activation energy of 11.4 kJ mol^{-1} is comparable to that for noncatalytic $^{3}\mathbf{2}$ formation (12.2 kJ mol^{-1}). The decrease of negative spin density on the alkoxy radical O(2) atom from −0.82 to 0.00, and shortening of the O(2)−C(2) bond length from 1.350 Å to 1.213 Å show that the formation of a formyl group proceeds by β-scission. The negative spin densities on C(2), and C(4) increase from −0.15 and −0.05 to −0.67 and −0.71, respectively, indicating the formation of an allyl radical with a C(1)−C(2) homolytic bond cleavage at $^{2}\mathbf{5}^{\mathbf{IV}}$. During this step, the spin densities of the Fe^{IV}-porphyrin system do not change much, indicating that the spin state of Fe^{IV} is unchanged. In the case of the Fe^{III} pathway, an allyl radical intermediate, $^{2}\mathbf{6}^{\mathbf{III}}$, forms with β-scission of the alkoxy radical as occurs in the formation of $^{2}\mathbf{6}^{\mathbf{IV}}$.

In the third step, the rotation of the formyl group in $^{2}\mathbf{6}^{\mathbf{IV}}$ and $^{2}\mathbf{6}^{\mathbf{III}}$ results in the formation of other allyl radical intermediates $^{2}\mathbf{7}^{\mathbf{IV}}$ and $^{2}\mathbf{7}^{\mathbf{III}}$ with an energy change of −6.9 kJ mol^{-1} and −7.1 kJ mol^{-1}, respectively. The Fe^{III}-porphyrin π-cation radical intermediates, $^{2}\mathbf{6}^{\mathbf{III}}$ and $^{2}\mathbf{7}^{\mathbf{III}}$, are higher in energy by 20 kJ mol^{-1} than the Fe^{IV} intermediates, $^{2}\mathbf{6}^{\mathbf{IV}}$ and $^{2}\mathbf{7}^{\mathbf{IV}}$ (Figure 7). Note that the quartet pathway from $^{4}\mathbf{5}^{\mathbf{IV}}$ to $^{4}\mathbf{7}^{\mathbf{IV}}$ through $^{4}\mathbf{6}^{\mathbf{IV}}$ is energetically similar to the doublet pathway. An Fe^{III} complex with a zwitterionic intermediate ($^{2}\mathbf{6}$) cannot be located at the UB3LYP/BII//UB3LYP/BI level, and leads to $^{2}\mathbf{6}^{\mathbf{IV}}$(Figure 10).[40]

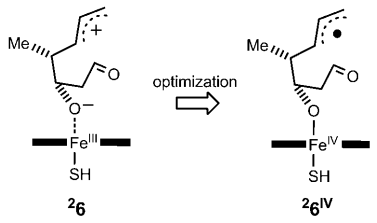

Figure 10. Trial for geometry optimization of zwitterionic Fe^{III} complex at the UB3LYP/BI level.

The binding of the carbonyl oxygen O(2) to the allyl carbon C(2) in the intermediate $^{2}\mathbf{7}^{\mathbf{IV}}$ leads to a six-membered ring oxanyl cation $^{2}\mathbf{8}$. The transition state between $^{2}\mathbf{7}^{\mathbf{IV}}$ and $^{2}\mathbf{8}$ could not be determined by conventional optimization techniques in the Gaussian 03 program arising from the discontinuity of the energy curve between $^{2}\mathbf{7}^{\mathbf{IV}}$ and $^{2}\mathbf{8}$ at the UB3LYP/BI level. Therefore, we performed a geometry scan to determine O(2)−C(2) distance. The resultant energy profile is summarized in Figure 11 at the UB3LYP/BII//

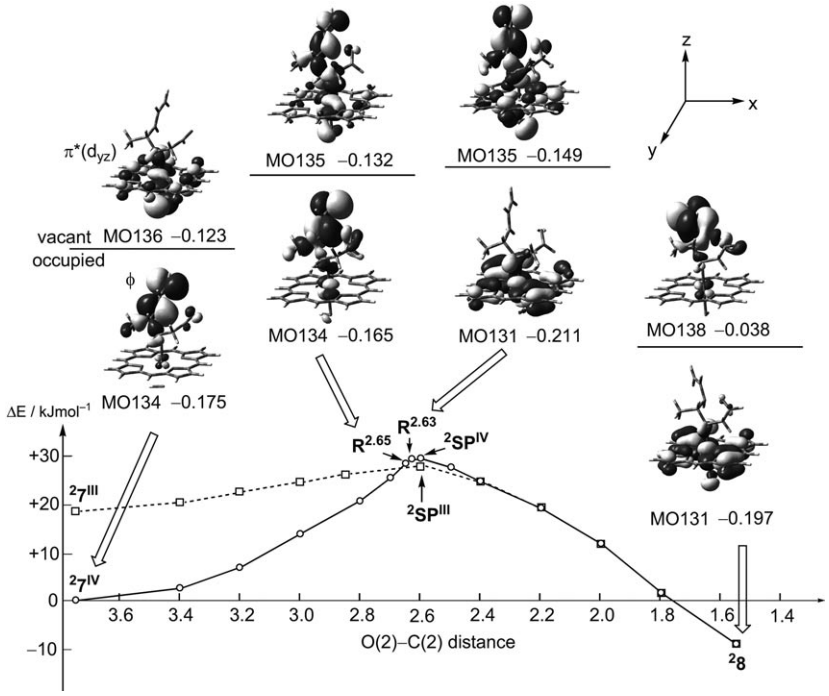

Figure 11. Geometry scans for the O(2)−C(2) bond formation at the UB3LYP/BII//UB3LYP/BI level and key β orbitals of the 6-membered ring formation at the UB3LYP/BI level. All energies for the scan are relative to the energy of $^{2}\mathbf{4}^{\mathbf{IV}}$. The numbers in the plain text indicate orbital energies in Hartree.

UB3LYP/BI level. The point ^{2}**SP^{IV}** in Figure 11 lies in the highest energy region at the UB3LYP/BII//UB3LYP/BI level along the energy curve. ^{2}**SP^{IV}** can be regarded as a transition state with six-membered ring formation. The activation energy is estimated to be 29.5 kJ mol^{-1}. Furthermore, we investigated the changes in the molecular orbitals of the geometries between ^{2}**7^{IV}** and ^{2}**8** at the UB3LYP/BI level. The key β-orbitals of representative points on the potential curve ^{2}**7^{IV}**, **R$^{2.65}$** (a point with a O(2)−C(2) distance of 2.65 Å), **R$^{2.63}$**(a point with a O(2)−C(2) distance of 2.63 Å), and ^{2}**8** are also illustrated in Figure 11. In ^{2}**7^{IV}**, the π*(d_{yz})-(MO136) orbital, which consists of d_{yz} (Fe), p (O(1)), and p (S) orbitals, is vacant and an allyl radical orbital φ (MO134) is occupied. With the shortening of the O(2)−C(2) bond length, these π* and φ orbitals further overlap (**R$^{2.65}$** in Figure 11). At the point of **R$^{2.63}$**, the order of energies of π* and φ orbitals are reversed, leading to occupied π* and vacant φ orbitals. As a result, ^{2}**8** vacates φ orbitals and occupies π* orbitals. Therefore, we conclude that the six-membered ring formation occurs with one electron transfer from the allyl group to Fe (Figure 12). In the ring closure process

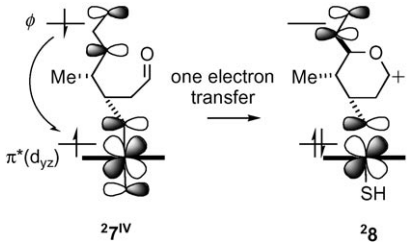

Figure 12. Schematic molecular orbital interaction of the one electron transfer from the allyl orbital (φ) to the iron d orbital (π*(d_{yz})).

from ^{2}**7^{IV}** to ^{2}**8**, the negative charge, by the natural population analysis of O(1), increases from −0.68 to −0.85, and that on C(1) decreases from +0.44 to +0.56. The spin density on Fe of 1.14 in ^{2}**8** indicates the low spin Fe^{III} state. These results show that ^{2}**8** can be classified as a complex of Fe^{III}-porphyrin with the zwitterionic substrate. Since the transition state between ^{2}**7^{III}** and ^{2}**8** could also not be located, a geometry scan for the O(2)−C(2) bond formation from the doublet Fe^{III} intermediate ^{2}**7^{III}** to ^{2}**8** was also performed (Figure 11). The highest energy region of the pathway from ^{2}**7^{III}** to ^{2}**8** through ^{2}**SP^{III}** is comparable to that of the pathway from ^{2}**7^{IV}** to ^{2}**8** through ^{2}**SP^{IV}**. The activation energy in the former pathway is estimated to be 9.5 kJ mol^{-1}. The activation energy of 102.7 kJ mol^{-1} for ^{3}**3** formation in the case of a noncatalytic reaction (see above) is much greater than the estimated activation energies of 29.5 kJ mol^{-1} and 9.5 kJ mol^{-1} for ^{2}**8** formation from ^{2}**7^{IV}** and ^{2}**7^{III}**, respectively. These results imply that the one electron transfer from the allyl group to Fe is essential to facilitate six-membered ring zwitterion formation, and that the six-membered ring zwitterion formation can occur throughout the Fe^{III} pathway if the Fe^{III}-porphyrin π-cation radical forms with an alkoxy radical ^{2}**7^{III}** forms. In case of a quartet state ^{4}**7^{IV}**, ring formation without one electron transfer leads to a 2-oxanyl radical Fe^{IV} intermediate ^{4}**8^{IV}**. The reactive intermediates with cationic or radical substrate depending on spin states, such as ^{2}**8** and ^{4}**8^{IV}**, have been already located in previous density functional studies on ethane epoxidation[32] and benzene hydroxylation[28] using the P450 model **A**, and on ethylbenzene hydroxylation by an oxo-iron-porphyrin catalyst [(Fe=O)Cl-(Por)].[37] These reports also show that the cationic complex is more stable than the radical complex.

Finally, the O(1)−C(1) bond formation of the zwitterionic intermediate ^{2}**8** leads to a complex of a model of TXA_2 (**C**) with **A**, ^{2}**PD1**, without any barrier. Even in the case of a noncatalytic reaction, the activation energy of noncatalytic **C** formation is 2.7 kJ mol^{-1} and is very low. The quartet pathway for the formation of the complex of the TXA_2 model with **A**, ^{4}**PD1**, from ^{4}**8^{IV}** through ^{4}**TS7^{IV}** is higher in energy than the doublet pathway. The fragmentation product ^{2}**PD2**, a complex of MDA and **D**, is formed by homolytic cleavage of the C(5)−C(6) bond through one transition state ^{2}**TS8^{IV}** from ^{2}**7^{IV}**, or through the other transition state ^{2}**TS8^{III}** from ^{2}**7^{III}**. The activation energy of 20.9 kJ mol^{-1} for fragmentation from ^{2}**7^{IV}** is lower than that of 29.5 kJ mol^{-1} for ^{2}**PD1** formation (Figure 7). The activation energies for fragmentation and TXA_2 formation may change if one investigates the free energy profile by using the whole enzyme model, and if one carries out detailed dynamics of one electron transfer process from **7** to **PD1**. The doublet pathway from ^{2}**7^{III}** through ^{2}**TS8^{III}** proceeds without any activation energy at the UB3LYP/BII//UB3LYP/BI level. The quartet fragmentation pathway from ^{4}**7^{IV}** to ^{4}**PD2** through ^{4}**TS8^{IV}** with an activation energy of 28.8 kJ mol^{-1} is higher in energy than the doublet Fe^{IV} fragmentation pathway of 20.9 kJ mol^{-1}.

Conclusions

As shown above, two reaction pathways through the Fe^{IV} intermediates or Fe^{III}-porphyrin π-cation radical intermediates were located by using density functional calculations. The overall reaction is exothermic, therefore TXA_2 formation should proceed spontaneously with a homolytic O−O bond cleavage. A very recent report on the endoperoxide isomerization reaction by a heme thiolate complex strongly supports the homolytic cleavage of the O−O bond.[41] Our results using model compounds show that the Fe^{III}-porphyrin π-cation radical intermediates are higher in energy by approximately 20 kJ mol^{-1} than the Fe^{IV}-porphyrin intermediates. A comparison between the energetics of C−H hydroxylation using model **A** with the aid of density functional theory, and the energetics of the reaction using the whole-enzyme model of cytochrome $P450_{cam}$ with the aid of the combined quantum mechanics/molecular mechanics (QM/MM) calculations, show that the protein environment reverses relative energies between the Fe^{III} and Fe^{IV} inter-

mediates, and lowers the energy for the Fe^{III} intermediates.[42] In the case of TXA_2 biosynthesis, the protein environment may make the Fe^{III}-porphyrin π-cation radical pathway more accessible by steric and electrostatic effects.

On the basis of the present results, we have proposed reaction mechanisms through two different oxidation states for thromboxane A_2 biosynthesis (Scheme 3). First, the endoperoxide oxygen atom at the C(9)-position of PGH_2 attaches to the heme iron of the TXAS active site. Next, an alkoxy radical intermediate is formed by O–O homolytic bond cleavage, followed by the formation of an allyl radical intermediate with C(11)–C(12) bond cleavage of the alkoxy radical intermediate. Finally, the formation of a 6-membered ring with one electron transfer leads to the production of TXA_2, and the homolytic cleavage of C(8)–C(9) bond competitively leads to fragmentation products (HHT and MDA). The proposed mechanism differs from the previous one with respect to the one electron transfer that occurs with the six-membered ring formation (see Schemes 2 and 3).

Our results showed some mechanistic insights into TXA_2 biosynthesis as follows. (i) The one electron transfer to the heme iron from the allyl group in the oxanyl ring formation step is essential to facilitate TXA_2 formation. In other words, TXA_2 formation requires an Fe^{III}-containing catalyst with one-electron acceptor ability. This situation is consistent with previous results,[15] which showed that TXA_2 cannot be produced with non-heme Fe^{II} catalysts. Not only Fe^{III}-containing catalysts but also other metal-containing catalysts with one-electron acceptor ability may catalyze TXA_2 formation.[43] (ii) The rate limiting step after PGH_2 binding to TXAS is the homolytic cleavage of the O–O bond in PGH_2.

The present study shows the mechanism of the isomerization reaction catalyzed by cytochrome P450, and the role of the heme-thiolate system. The results provided important insights into understanding the unusual reactions by P450, for example, PGI_2 biosynthesis.

Computational Methods

Reasonable model selection with satisfactory accuracy is essential for quantum mechanical studies. We used a model for P450, **A**, which consists of a porphyrin ring that represents protoporphyrin IX, and an SH ion that represents the cysteine residue. This model, **A**, has been studied by Shaik and co-workers, and gave satisfactory results in the gas-phase,[36] and is a good model for the cytochrome P450 active site.[44] In the model for PGH_2, **B**, two side chains were replaced with methyl and vinyl groups (Figure 2). All calculations in the present study were performed with the Gaussian 03 program,[45] and by using the symmetry-broken unrestricted Becke-three-parameter plus Lee–Yang–Parr (UB3LYP) DFT method.[26] The B3LYP functional is able to provide a satisfactory description for structures and energetics of the iron-containing system.[36,46] For all geom-

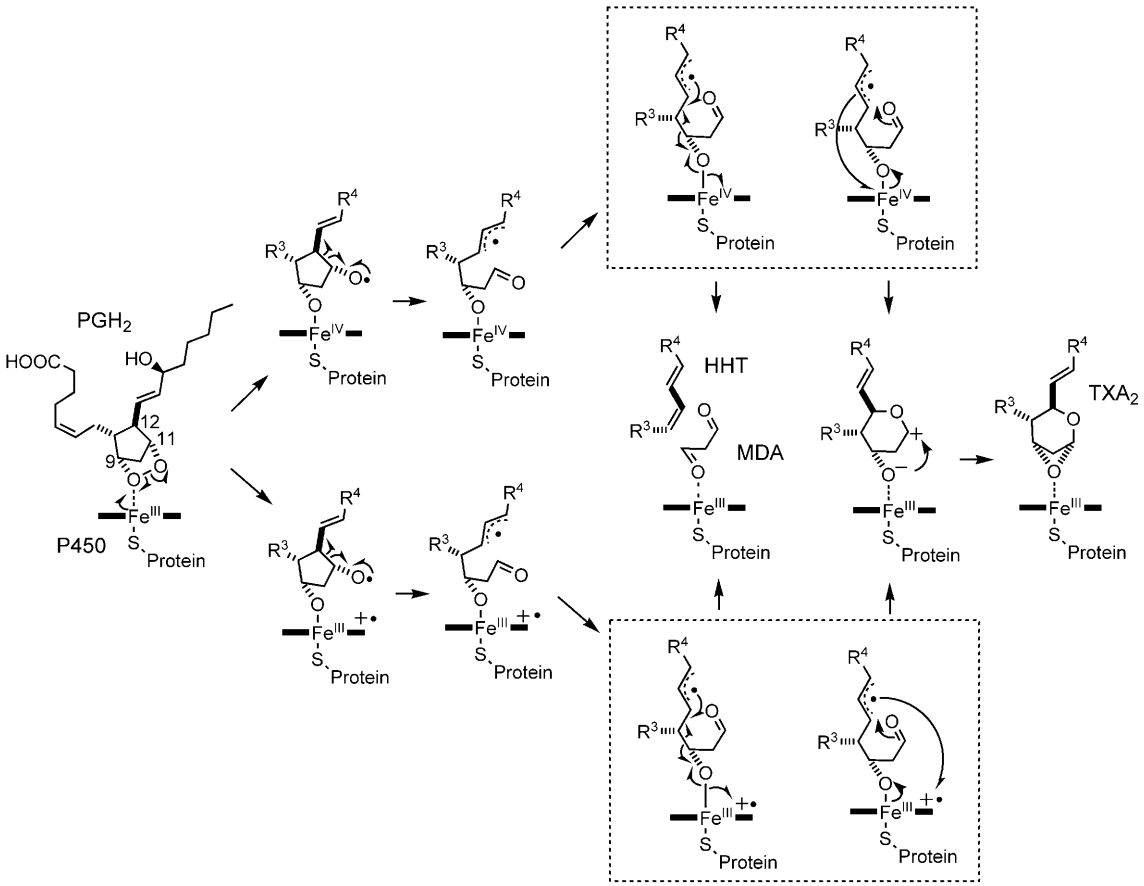

Scheme 3. Newly proposed reaction mechanism of TXA_2 biosynthesis.

etry optimizations, and normal coordinate analyses at stationary points, we used LANL2DZ effective core potential with a basis set for Fe,[47] 6-31G(d) basis set for all atoms in the PGH_2 model **B**, N atoms, and the SH group, and 3-21G basis set for the others. This basis set combination is termed BI in this paper. We also optimized the model **A** with a larger basis set, BII (quasi-relativistic Stuttgart–Dresden–Cologne (SDD) effective core potential with one f function of exponent $\alpha = 10.035$ basis set[48] for Fe, and 6-311+G(d) for the others). No significant change was confirmed on bond distances and spin densities at the UB3LYP/BII//UB3LYP/BII level compared to the UB3LYP/BI level (details are provided as Figure S4 and Scheme S1, Supporting Information), hence the BI basis set was employed for geometry optimization. In single point energy calculations, we used the BII basis set. Doublet ($S = 1/2$: S refers to total spin angular momentum), quartet ($S = 3/2$), and sextet ($S = 5/2$) open-shell systems were considered. To investigate a reaction mechanism of the isomerization reaction from the PGH_2 model, **B**, to the TXA_2 model, **C**, in the absence of the iron-porphyrin **A**, we used the UB3LYP/BI method for geometry optimizations, subsequent normal coordinated analyses for the stationary points, and the UB3LYP/BII method for the single point energy calculations of UB3LYP/BI optimized structures. The molecular orbitals in Figure 11 were visualized using GaussView 3.0[49] Natural charges are computed with the NBO 5.G program.[50]

Acknowledgements

This work was supported by Grants-in-Aid No. 19550004 for Scientific Research from JSPS, and by Scientific Research on Priority Areas "Molecular Theory for Real Systems", No. 20038005 from MEXT. The generous allotment of computational time from the Research Center for Computational Science (RCCS), the National Institutes of Natural Sciences, Japan, is also gratefully acknowledged. We express our deep appreciation to Dr. Robert K. Szilagyi, Montana State University, for his generous help. We thank Prof. Tsunehiko Higuchi of Nagoya City University for preprints before publication.

[1] a) M. L. Ogletree, *Fed. Proc.* **1987**, *46*, 133–138; b) V. Ullrich, M.-H. Zou, M. Bachschmid, *Biochim. Biophys. Acta Mol. Cell Biol. Lipids* **2001**, *1532*, 1–14.

[2] a) S. Moncada, J. R. Vane, *Pharmacol. Rev.* **1978**, *30*, 293–331; b) J. R. Vane, R. M. Bonting, *Am. J. Cardiol.* **1995**, *75*, 3A-10A.

[3] a) P. V. Halushka, R. C. Rogers, C. B. Loadholt, J. A. Colwell, *J. Lab. Clin. Med.* **1981**, *97*, 87–96; b) S. J. Coker, J. R. Parratt, I. M. Ledingham, I. J. Zeitlin, *Nature* **1981**, *291*, 323–324; c) S. Bunting, S. Moncada, J. R. Vane, *Br. Med. Bull.* **1983**, *39*, 271–276; d) J. L. Mehta, D. Lawson, P. Mehta, T. Saldeen, *Proc. Natl. Acad. Sci. USA* **1988**, *85*, 4511–4515.

[4] a) V. Ullrich, H. Graf, *Trends Pharmacol. Sci.* **1984**, *5*, 352–355; b) P. Needleman, J. Turk, B. A. Jakschik, A. R. Morison, J. B. Lefkowith, *Annu. Rev. Biochem.* **1986**, *55*, 69–102.

[5] M. Haurand, V. Ullrich, *J. Biol. Chem.* **1985**, *260*, 15059–15067.

[6] U. Diczfalusy, P. Falardeau, S. Hammarström, *FEBS Lett.* **1977**, *84*, 271–274.

[7] R.-F. Shen, H.-H. Tai, *J. Biol. Chem.* **1986**, *261*, 11592–11599.

[8] a) *Cytochrome P450: Structure, Mechanism and Biochemistry, 3rd ed.* (Ed.: P. R. Ortiz de Montellano), Kluwer Academic/Plenum Publishers, New York, **2004**; b) M. Sono, M. P. Roach, E. D. Coulter, J. H. Dawson, *Chem. Rev.* **1996**, *96*, 2841–2887; c) J. H. Dawson, M. Sono, *Chem. Rev.* **1987**, *87*, 1255–1276; d) L. G. Denisov, T. M. Makrins, S. G. Sligar, I. Schlichting, *Chem. Rev.* **2005**, *105*, 2253–2277; e) F. P. Guengerich, *Chem. Res. Toxicol.* **2001**, *14*, 611–650; f) T. Omura, *Biochem. Biophys. Res. Commun.* **1999**, *266*, 690–698; g) A. W. Munro, H. M. Girvan, K. J. McLean, *Nat. Prod. Rep.* **2007**, *24*, 585–609.

[9] I. Schlichting, J. Berendzen, K. Chu, A. M. Stock, S. A. Maves, D. E. Benson, R. M. Sweet, D. Ringe, G. A. Petsko, S. G. Sliger, *Science* **2000**, *287*, 1615–1622.

[10] a) B. Pereira, K. K. Wu, L. H. Wang, *Biochem. Biophys. Res. Commun.* **1994**, *203*, 59066; b) S. Hara, A. Miyata, C. Yokoyama, H. Inoue, R. Brugger, F. Lottspeich, V. Ullrich, T. Tanabe, *J. Biol. Chem.* **1994**, *269*, 19897–19903.

[11] a) M. Hamberg, J. Svensson, B. Samuelsson, *Proc. Natl. Acad. Sci. USA* **1975**, *72*, 2994–2998; b) M. Hamberg, B. Samuelsson, *Proc. Natl. Acad. Sci. USA* **1974**, *71*, 3400–3404; c) M. Hamberg, J. Svensson, B. Samuelsson, *Proc. Natl. Acad. Sci. USA* **1974**, *71*, 3824–3828.

[12] a) B. Samuelsson, M. Goldyne, E. Granstrom, S. Hammarström, C. Malmsten, *Annu. Rev. Biochem.* **1978**, *47*, 997–1029; b) L.-H. Wang, R. J. Kulmacz, *Prostaglandins Other Lipid Mediators* **2002**, *68–69*, 409–422; c) V. Ullrich, R. Brugger, *Angew. Chem.* **1994**, *106*, 1987–1996; *Angew. Chem. Int. Ed. Engl.* **1994**, *33*, 1911–1919; d) T. Tanabe, V. Ullrich, *J. Lipid Mediators Cell Signalling* **1995**, *12*, 243–255; e) K.-H. Ruan, *Mini-Rev. Med. Chem.* **2004**, *4*, 639–647; f) S.-P. So, D. Li, J.-H. Ruan, *J. Biol. Chem.* **2000**, *275*, 40679–40685; g) K.-H. Ruan, J. Wu, L.-H. Wang, *Arch. Biochem. Biophys.* **2005**, *444*, 165–173.

[13] J. A. Turner, W. Herz, *Experientia* **1977**, *33*, 1133–1134.

[14] U. Diczfalusy, S. Hammarström, *Adv. Prostaglandin Thromboxane Res.* **1980**, *6*, 267–274.

[15] M. Hecker, V. Ullrich, *J. Biol. Chem.* **1989**, *264*, 141–150.

[16] P.-Y. Hsu, A.- L. Tsai, R. J. Kulmacz, L.-H. Wang, *J. Biol. Chem.* **1999**, *274*, 762–769.

[17] Z. Chen, L.-H. Wang, J. P. M. Schelvis, *Biochemistry* **2003**, *42*, 2542–2551.

[18] J. K. Kochi, in *Organometallic Mechanisms and Catalysis*, Academic Press, New York, **1978**, pp. 50–83.

[19] a) R. Labeque, L. J. Marnett, *J. Am. Chem. Soc.* **1989**, *111*, 6621–6627; b) S. E. J. Bell, P. R. Cooke, P. Inchley, D. R. Leanord, J. R. Lindsay Smith, A. Robbins, *J. Chem. Soc. Perkin Trans. 2* **1991**, 549–559; c) T. Higuchi, K. Shimada, N. Maruyama, M. Hirobe, *J. Am. Chem. Soc.* **1993**, *115*, 7551–7552; d) M. A. Correia, K. Yao, A. J. Allentoff, S. A. Wrighton, J. A. Thompson, *J. Biol. Chem.* **1995**, *317*, 471–478; e) O. Almarsson, T. C. Bruice, *J. Am. Chem. Soc.* **1995**, *117*, 4533–4544; f) F. Minisci, F. Fontana, S. Araneo, F. Recupero, S. Banfi, S. Quici, *J. Am. Chem. Soc.* **1995**, *117*, 226–232; g) D. P. Barr, M. V. Martin, F. P. Guengerich, R. P. Mason, *Chem. Res. Toxicol.* **1996**, *9*, 318–325; h) W. Nam, H. J. Han, S.-Y. Oh, Y. J. Lee, M.-H. Choi, S.-Y. Han, C. Kim, S. K. Woo, W. Shin, *J. Am. Chem. Soc.* **2000**, *122*, 8677–8684.

[20] H.-C. Yeh, A.- L. Tsai, L.-H. Wang, *Arch. Biochem. Biophys.* **2007**, *461*, 159–168.

[21] H.-C. Yeh, P.-Y. Hsu, J.-S. Wang, A.- L. Tsai, L.-H. Wang, *Biochim. Biophys. Acta* **2005**, *1738*, 121–132.

[22] L.-H. Wang, A.- L. Tsai, P.-Y. Hsu, *J. Biol. Chem.* **2001**, *276*, 14737–14743.

[23] a) Z. Xia, R.-F. Shen, S. J. Baek, H.-H. Tai, *Biochem. J.* **1993**, *295*, 457–461; b) L.-H. Wang, N. Matijevic-Aleksic, P.-Y. Hsu, K.-H. Ruan, K. K. Wu, R. J. Kulmacz, *J. Biol. Chem.* **1996**, *271*, 19970–19975; c) P.-Y. Hsu, A.- L. Tsai, L.-H. Wang, *Arch. Biochem. Biophys.* **2000**, *383*, 119–127.

[24] K.-H. Ruan, K. Milfeld, R. J. Kulmacz, K. K. Wu, *Protein Eng.* **1994**, *7*, 1345–1351.

[25] a) C.-W. Chiang, H.-C. Yeh, L.-H. Wang, N.- L. Chan, *J. Mol. Biol.* **2006**, *364*, 266–274; b) Y.-C. Li, C.-W. Chiang, H.-C. Yeh, P.-Y. Hsu, F. G. Whitby, L.-H. Wang, N.- L. Chan, *J. Biol. Chem.* **2008**, *283*, 2917–2926.

[26] a) A. D. Becke, *J. Chem. Phys.* **1993**, *98*, 5648—5652; b) C. Lee, W. Yang, R. G. Parr, *Phys. Rev. B* **1988**, *37*, 785–789.

[27] a) M. Filatov, N. Harris, S. Shaik, *Angew. Chem.* **1999**, *111*, 3730–3733; *Angew. Chem. Int. Ed.* **1999**, *38*, 3510–3512; b) M. Filatov, N. Harris, S. Shaik, *J. Chem. Soc. Perkin Trans. 2* **1999**, 399–410; c) N. Harris, S. Cohen, M. Filatov, F. Ogliaro, S. Shaik, *Angew. Chem.* **2000**, *112*, 2070–2074; *Angew. Chem. Int. Ed.* **2000**, *39*, 2003–2007; d) K. Yoshizawa, Y. Shiota, Y. Kagawa, *Bull. Chem. Soc. Jpn.* **2000**,

73, 2669–2673; e) K. Yoshizawa, T. Ohta, M. Eda, T. Yamabe, *Bull. Chem. Soc. Jpn.* **2000**, *73*, 401–407; f) F. Ogliaro, N. Harris, S. Cohen, M. Filatov, S. P. de Visser, S. Shaik, *J. Am. Chem. Soc.* **2000**, *122*, 8977–8989; g) O. Zakharieva, A. X. Trautwein, C. Veeger, *Biophys. Chem.* **2000**, *88*, 11–34; h) C. M. Bathelt, L. Ridder, A. J. Mulholland, J. N. Harvey, *J. Am. Chem. Soc.* **2003**, *125*, 15004–15005; i) T. Kamachi, K. Yoshizawa, *J. Am. Chem. Soc.* **2003**, *125*, 4652–4661; j) V. Guallar M.-H. Baik S. J. Lippard R. A. Friesner, *Proc. Natl. Acad. Sci. USA* **2003**, *100*, 6998–7002; k) D. Kumar, S. P. de Visser, S. Shaik, *J. Am. Chem. Soc.* **2003**, *125*, 13024–13025; l) M. Hata, Y. Hirano, T. Hoshino, R. Nishida, M. Tsuda, *J. Phys. Chem. B.* **2004**, *108*, 11189–11195; <lit m>Y. K. Choe, S. Nagase, *J. Comput. Chem.* **2005**, *26*, 1600–1611; n) C. Li, W. Wu, D. Kumar, S. Shaik, *J. Am. Chem. Soc.* **2006**, *128*, 394–395; o) Y. Wang, H. Wang, Y. Wang, C. Yang, L. Yang, K. Han, *J. Phys. Chem. B* **2006**, *110*, 6154–6159; p) R. D. Bach, O. Dmitrenko, *J. Am. Chem. Soc.* **2006**, *128*, 1474–1488; q) L. Olsen, P. Rydberg, T. H. Rod, U. Ryde, *J. Med. Chem.* **2006**, *49*, 6489–6499; r) X. Liu, Y. Wang, K. Han, *J. Biol. Inorg. Chem.* **2007**, *12*, 1073–1081; s) M. Shoji, H. Isobe, T. Saito, H. Yabushita, K. Koizumi, Y. Kitagawa, S. Yamanaka, T. Kawakami, M. Okumura, M. Hagiwara, K. Yamaguchi, *Int. J. Quantum Chem.* **2008**, *108*, 631–650.

[28] S. P. de Visser, S. Shaik, *J. Am. Chem. Soc.* **2003**, *125*, 7413–7424.

[29] a) S. P. de Visser, F. Ogliaro, P. K. Sharma, S. Shaik, *J. Am. Chem. Soc.* **2002**, *124*, 11809–11826; b) S. P. de Visser, D. Kumar, S. Cohen, R. Shacham, S. Shaik, *J. Am. Chem. Soc.* **2004**, *126*, 8362–8363; c) D. Kumar, S. P. de Visser, P. K. Sharma, S. Cohen, S. Shaik, *J. Am. Chem. Soc.* **2004**, *126*, 1907–1920.

[30] a) H. Hirao, D. Kumar, W. Thiel, S. Shaik, *J. Am. Chem. Soc.* **2005**, *127*, 13007–13018; b) K. Yoshizawa, Y. Kagawa, Y. Shiota, *J. Phys. Chem. B* **2000**, *104*, 12365–12370.

[31] a) S. P. de Visser, F. Ogliaro, N. Harris, S. Shaik, *J. Am. Chem. Soc.* **2001**, *123*, 3037–3047; b) S. P. de Visser, F. Ogliaro, S. Shaik, *Angew. Chem.* **2001**, *113*, 2955–2958; *Angew. Chem. Int. Ed.* **2001**, *40*, 2871–2874; c) F. Ogliaro, S. P. de Visser, S. Cohen, P. K. Sharma, S. Shaik, *J. Am. Chem. Soc.* **2002**, *124*, 2806–2817.

[32] S. P. de Visser, D. Kumar, S. Shaik, *J. Inorg. Biochem.* **2004**, *98*, 1183–1193.

[33] P. K. Sharma, S. P. de Visser, S. Shaik, *J. Am. Chem. Soc.* **2003**, *125*, 8698–8699.

[34] Y. Wang, D. Kumar, C. Yang, K. Han, S. Shaik, *J. Phys. Chem. B* **2007**, *111*, 7700–7710.

[35] a) M. A. Vincent, I. H. Hillier, J. Ge, *Chem. Phys. Lett.* **2005**, *407*, 333–336; b) N. Lehnert, V. K. K. Praneeth, F. Paulat, *J. Comput. Chem.* **2006**, *27*, 1338–1351.

[36] S. Shaik, D. Kumar, S. P. de Visser, A. Altun, W. Thiel, *Chem. Rev.* **2005**, *105*, 2279–2328.

[37] S. P. de Visser, *Chem. Eur. J.* **2006**, *12*, 8168–8177.

[38] Even though the active site of TXAS is highly hydrophobic (Ref. [16]), we estimated activation energies with solvent effect in case. Single point energy calculations using the conductor-like polarized continuum method (CPCM) with mild dielectric constant of 5.7 (see Ref. [32]) at the UB3LYP/BII//UB3LYP/BI level showed that the doublet state ^{2}**4** is *higher* in energy than the quartet state ^{4}**4** by 8.6 kJ mol^{-1}. The energetic trend at the UB3LYP(CPCM)/BII//UB3LYP/BI level is not consistent with the experimental evidences. The details are provided as Figure S3 in the Supporting Information. For the CPCM method, see : V. Barone, M. Cossi, *J. Phys. Chem. A* **1998**, *102*, 1995–2001.

[39] T. L. Poulos, B. C. Finzel, A. J. Howard, *Biochemistry* **1986**, *25*, 5314–5322.

[40] We evaluated a wave function of the zwitterion complex using the ^{2}**6**^{IV} geometry with an allyl radical by using the generalized ionic fragment approach (GIFA), which is helpful in development of several electronic states, and performed geometry optimization at the B3LYP level. However, the zwitterion complex cannot be located. Reference of the GIFA: R. K. Szilagyi, M. Winslow, *J. Comput. Chem.* **2006**, *27*, 1385–1397.

[41] T. Yamane, K. Makino, N. Umezawa, N. Kato, T. Higuchi, *Angew. Chem.* **2008**, *120*, 6538–6540; *Angew. Chem. Int. Ed.* **2008**, *47*, 6438–6440.

[42] J. C. Schöneboom, S. Cohen, H. Lin, S. Shaik, W. Thiel, *J. Am. Chem. Soc.* **2004**, *126*, 4017–4034.

[43] Although the mechanism is not clear, Fe^{II} promotes degradation of related cyclic peroxides. See: M. Kamata, M. Ohta, K.-i. Komatsu, H.-S. Kim, Y. Wataya, *Tetrahedron Lett.* **2002**, *43*, 2063–2067. See also Ref. [13].

[44] J. C. Schöneboom, N. Reuter, H. Lin, W. Thiel, S. Cohen, F. Ogliaro, S. Shaik, *J. Am. Chem. Soc.* **2002**, *124*, 8142–8151.

[45] *Gaussian 03, Revision D.02*, M. J. Frisch, G. W. Trucks, H. B. Schlegel, G. E. Scuseria, M. A. Robb, J. R. Cheeseman, J. A. Montgomery, Jr., T. Vreven, K. N. Kudin, J. C. Burant, J. M. Millam, S. S. Iyengar, J. Tomasi, V. Barone, B. Mennucci, M. Cossi, G. Scalmani, N. Rega, G. A. Petersson, H. Nakatsuji, M. Hada, M. Ehara, K. Toyota, R. Fukuda, J. Hasegawa, M. Ishida, T. Nakajima, Y. Honda, O. Kitao, H. Nakai, M. Klene, X. Li, J. E. Knox, H. P. Hratchian, J. B. Cross, V. Bakken, C. Adamo, J. Jaramillo, R. Gomperts, R. E. Stratmann, O. Yazyev, A. J. Austin, R. Cammi, C. Pomelli, J. W. Ochterski, P. Y. Ayala, K. Morokuma, G. A. Voth, P. Salvador, J. J. Dannenberg, V. G. Zakrzewski, S. Dapprich, A. D. Daniels, M. C. Strain, O. Farkas, D. K. Malick, A. D. Rabuck, K. Raghavachari, J. B. Foresman, J. V. Ortiz, Q. Cui, A. G. Baboul, S. Clifford, J. Cioslowski, B. B. Stefanov, G. Liu, A. Liashenko, P. Piskorz, I. Komaromi, R. L. Martin, D. J. Fox, T. Keith, M. A. Al-Laham, C. Y. Peng, A. Nanayakkara, M. Challacombe, P. M. W. Gill, B. Johnson, W. Chen, M. W. Wong, C. Gonzalez, and J. A. Pople, Gaussian, Inc., Wallingford, CT, USA, **2004**.

[46] a) M.-S. Liao, J. D. Watts, M.- J. Huang, *J. Comput. Chem.* **2006**, *27*, 1577–1592; b) P. E. M. Siegbahn, T. Borowski, *Acc. Chem. Res.* **2006**, *39*, 729–738.

[47] P. J. Hay, W. R. Wadt, *J. Chem. Phys.* **1985**, *82*, 299–310.

[48] M. Dolg, U. Wedig, H. Stoll, H. Preuss, *J. Chem. Phys.* **1987**, *86*, 866–872.

[49] GaussView, Version 3.0, R. Dennington II, T. Keith, J. Millam, K. Eppinnett, W. L. Hovell, R. Gilliland, Semichem, Inc., Shawnee Mission, KS, USA, **2003**.

[50] NBO Version 5.G implemented by E. D. Glendening, A. E. Reed, J. E. Carpenter, F. Weinhold, **2005**.

Received: July 4, 2008
Published online: October 10, 2008

